

Reconstruction and approximation effects on W mass distributions at LEP2. ¹

Alessandro Ballestrero^{ab} and Roberto Chierici^{ac}

^a*I.N.F.N., Sezione di Torino, v. Giuria 1, 10125 Torino, Italy*

^b*Dipartimento di Fisica Teorica, Università di Torino, Italy*

^c*Dipartimento di Fisica Sperimentale, Università di Torino, Italy.*

Abstract

We analyze from a theoretical point of view the impact of various approximations on W mass distributions. This is done both at parton level and after a simulated W mass reconstruction using constrained fits. The results may help to understand the origin of various shifts and the broadening of the peak in direct reconstruction mass measurements.

¹ Work supported in part by Ministero dell' Università e della Ricerca Scientifica.
e-mail: ballestrero@to.infn.it, chierici@to.infn.it

1 Introduction.

One of the main purposes of LEP2 physics is the measurement of the W mass [1]. The combined theoretical and experimental effort will hopefully lead to its determination with an accuracy of the order of 50 MeV. After the threshold measurements at 161 GeV [2], in the runs at higher energies the so called direct reconstruction method will be used. The first results at 172 GeV have already been reported by LEP collaborations [3][4]. The above method is based on the determination of the invariant mass of the two couples of fermions coming from the decay of the W's intermediate states. This is complicated by the initial state radiation (ISR), by the presence of the invisible neutrinos in semileptonic channels and by the experimental difficulty of reconstructing the invariant mass of two jets. For this reason kinematical constrained fits to the measured four-momenta are used, in order to improve the resolution on the invariant mass [3][4]. Another difficulty comes from the fact that not only the three double resonant diagrams (CC3) contribute to the four fermion final states, but also other diagrams which represent the so called irreducible background. For instance the typical four quarks charged current process $u\bar{d}s\bar{c}$ (CC11) is composed of 11 diagrams and the semileptonic $e\bar{\nu}u\bar{d}$ (CC20) by 20. Moreover, as the light quark flavour is practically indistinguishable, all four quark final states have to be accounted for and not only those coming from charged currents. Many theoretical groups have produced programs to compute four fermion processes (for a review of these generators, see [5]). Some of these programs can compute all possible processes and a complete analysis of the various contributions to invariant mass distributions has already been performed [6].

In this letter we want to consider some of the most relevant approximations and uncertainties which are often unavoidable in the simulations and in the direct reconstruction method. In particular we want to study their effect both at the parton level and after a simulated reconstruction procedure in order to understand their relative importance on mass shifts and distributions broadening. We do this with the help of WPHACT [7], one of the complete four fermion codes. To simulate the reconstruction, we use a smearing of the theoretical four momenta produced by WPHACT with a procedure inspired by ref. [4] and then we pass them to the constrained fit program PUFITC (for a description of the fitting technique see again ref. [4]). The resulting distributions at generator (WPHACT) level and after the simulated reconstruction are analyzed and fitted with a Breit Wigner (BW) to determine a measure of the mass shifts and broadenings.

The plan of the paper is the following: in section 2 we give some details on the distributions, their BW fits and estimated errors. In section 3 we analyze the theoretical distributions at generator level. Section 4 is dedicated to an explanation of smearing and constrained fit procedure. The results for the distributions and the parameters obtained in this way are discussed in section 5. Some conclusions are drawn in section 6.

For the numerical part we have chosen as input parameters:

$$m_W = 80.356 \text{ GeV}, \quad m_Z = 91.888 \text{ GeV}, \quad s_w^2 = 1 - \frac{m_W^2}{m_Z^2}, \quad g^2 = 4\sqrt{2}G_\mu m_W^2.$$

The only cuts applied at parton level are those on the angle of each fermion with respect to the beam, which we have required to be greater than 10 degrees. Other cuts after momentum smearing are described in sect. 4.

2 Distributions and their fit.

All distributions were produced using WPHACT with a binning of 100 MeV and a relative accuracy per bin of a few per mill. To assess the differences between mass distributions, we fitted them with a Breit-Wigner corresponding to a running width W propagator squared:

$$BW(m; m_W, \Gamma, N) = \frac{N}{(m^2 - m_W^2)^2 + (\Gamma m^2/m_W)^2}, \quad (1)$$

where m_W , Γ and N are the three parameters of our χ^2 fit.

The difference between the values of the fitted BW masses and widths of two curves can be considered as an indication of their relative distortion.

All fits were performed with PAW [8] in the interval 78 - 82.5 GeV. Such an interval was chosen in order not to fit the tails of the distributions, where phase space and matrix element effects are stronger.

The χ^2/dof 's obtained from the fit were generally bad. This is due to the smallness of the errors on the distributions and the fact that the Breit-Wigner curve is a very simple approximation to the differential cross-sections $d\sigma/dm$. This is confirmed by the sensitivity of the parameters to the width of the interval chosen. Varying it, for instance, to 78 - 82 GeV, produces a variation on the fitted mass of some MeV.

We therefore conservatively associate an error to the fitted values of m and Γ which is rescaled with respect to the one given by PAW, by a factor $\sqrt{\chi^2/dof}$. With such a procedure we obtain a maximum error of 5 MeV for the mass. As far as the width is concerned, one gets a maximum error of 15 MeV for parton level distributions and 25 MeV for the others. These errors are however overestimated by about a factor 3 if they refer to the definite interval used. From now on it must be understood that the numerical results are affected by such uncertainties.

With these provisos we believe that our fitted values and especially their differences can be considered good estimates of the shifts and broadenings.

3 Parton level analysis of some approximations and constraints.

We study in this section the relevance on parton level computations of some approximations and constraints which are sometimes used in simulations or in the reconstruction of the W mass from experimental data. We examine, for instance, the effect of neglecting ISR or that of computing only the CC3 subset of diagrams. Such computations

have already been performed many times in the literature [6][9][5][10]. However we do not simply apply them to total cross sections, but to invariant mass distributions, in order to understand how the above approximations affect their maximum, width and eventually their shape.

Let us start considering CC3 with and without ISR. An example of these distributions is reported in fig. 1.

The results of BW fits are reported in table 1.

	172 GeV		184 GeV		200 GeV	
	m_W	Γ	m_W	Γ	m_W	Γ
no ISR	80.320	2.062	80.377	2.087	80.397	2.091
ISR	80.296	2.060	80.364	2.091	80.389	2.096

Table 1: CC3 masses and widths (in MeV) with and without ISR for the average distributions.

They refer to the distribution of the mean value of the two reconstructed masses event by event. We will name it in the following average distribution, and it must not be confused with the one obtained taking the average of the two (e.g $m(e\bar{\nu})$ and $m(u\bar{d})$) invariant mass distributions. One notices a deviation of the fitted masses from the input value $m_W = 80.356$ GeV. At 172 GeV the values are lower and this might be explained by the vicinity of the kinematical limit, while they become larger at higher energies. The shift due to ISR is of the order of 25 MeV at 172 GeV and it decreases to 8 MeV at higher energies. There is practically no effect on the width. Coming back to fig 1, one may then say that the major effect at the parton level of ISR on mass distributions is to lower them: this can also be proven by normalizing the two curves to the same value and superimposing them.

There are other ways in which ISR influences the mass measurements. In the semileptonic final states, the neutrino is invisible and its momentum can be only approximately reconstructed. The best way to do it is to attribute all missing three momentum \vec{p}_{mis} to the neutrino and take its energy to be equal to the modulus $|\vec{p}_{mis}|$. This method, which would of course be exact in case of no initial state radiation, leads to a distortion of the mass distribution. An example of this effect is shown in fig. 2. In table 2 are reported the results obtained fitting with a BW $m(e\bar{\nu})$ and average distributions. m and Γ are the parameters resulting from fits with exact neutrino momenta. Δm and $\Delta\Gamma$ are the differences between the previous ones and those from fits to reconstructed neutrino distributions.

The results of the table show clearly that the shift for this reconstructed momentum effect is of the order of 20 MeV, not dependent on the energy. The width is enlarged of about 10%.

In practice these reconstructed mass distributions are never used: the reconstructed neutrino momentum is normally an input of a fit procedure in which the conservation of the energy and the equality of the leptonic and hadronic invariant masses are used as constraints. It is well known that in reality the two invariant masses are not equal event

	172 GeV				184 GeV				200 GeV			
	m	Γ	Δm	$\Delta\Gamma$	m	Γ	Δm	$\Delta\Gamma$	m	Γ	Δm	$\Delta\Gamma$
$e\bar{\nu}$	80376	2096	19	255	80408	2100	19	326	80417	2101	18	364
Av	80340	2074	24	180	80405	2104	25	269	80426	2108	24	322

Table 2: Masses, widths and their differences (in MeV) between results from reconstructed and exact neutrino momenta. The data refer to CC20 $e\bar{\nu}$ and average invariant mass distributions.

by event. If we compute the distribution corresponding to the difference between $e\bar{\nu}$ and $u\bar{d}$ invariant masses in $e\bar{\nu}u\bar{d}$ final state at 172 GeV, one finds [11] that its maximum at zero is about 1 pb, and its width at half height is about 4 GeV. The width of the two BW's, the contribution of non resonant diagrams and kinematic effects produce such difference. Nevertheless, requiring equal masses in the fit represents an approximation which is useful to improve considerably the mass resolution [1].

We want now to understand how using complete calculations instead of double resonant diagrams only, reflects on fitted masses and widths. To this end we have performed the fit on CC3 and CC20 distributions and we report the results in table 3.

	172 GeV				184 GeV				200 GeV			
	m	Γ	Δm	$\Delta\Gamma$	m	Γ	Δm	$\Delta\Gamma$	m	Γ	Δm	$\Delta\Gamma$
$u\bar{d}$	80332	2089	-4	-2	80366	2096	-3	1	80379	2098	0	0
$e\bar{\nu}$	80331	2090	44	6	80366	2096	42	4	80380	2097	37	3
Av	80296	2060	44	14	80364	2091	41	13	80389	2096	37	12

Table 3: CC3 masses, widths and differences between CC20 and CC3 values (in MeV). The data refer $e\bar{\nu}$, $u\bar{d}$ and average invariant mass distributions.

We do not show a similar table to compare CC11 versus CC3, simply because the fitted values of masses and widths given by CC11 and CC3 are always within their estimated errors. The same applies to CC10 ($\mu\bar{\nu}u\bar{d}$). One immediately notices from table 3 that also Δm 's and $\Delta\Gamma$'s for quark distributions are irrelevant. The sizeable shift is on Δm 's for $e\bar{\nu}$ distribution. It is of the order of 40 MeV and it is amazing that it practically reflects entirely on the average distribution. From fig. 3 one realizes that the reason of the shift between CC20 and CC3 is completely due to interference effects. The interference between the double resonant diagrams and the diagrams which are obtained from the CC10 ones with the exchange of incoming e^+ with outgoing e^- , has only one W^- propagator. These contributions change sign when $m(e\bar{\nu})$ passes through m_W . For such a reason they depress masses lower than m_W and enhance the higher ones, thus leading to the shift. This implicitly makes us understand why CC20 $m(u\bar{d})$ and CC10 or CC11, which are not affected by such contributions, do not have a sizeable shift with respect to CC3.

4 Kinematic reconstruction of the event: its effect on the mass distribution.

To investigate the effects of a kinematic reconstruction of the W resonance, the four-momenta generated with WPHACT were first smeared to reproduce detector inefficiencies and hadronization effects and then used in a constrained fit to simulate an experimental determination of m_W . The smearing applied to three-momentum of the i -th quark was inspired by [4] and can be written as:

$$\vec{p}_s^i = e^a \vec{p}_g^i + b \vec{p}_{perp,1}^i + b \vec{p}_{perp,2}^i \quad (2)$$

where the subscripts s and g indicate respectively the smeared momenta and the generated ones; $\vec{p}_{perp,1}^i$ and $\vec{p}_{perp,2}^i$ are two vectors orthogonal to \vec{p}_g^i with random orientations. The variables a and b are random factors distributed according to gaussians with central values a_0 , b_0 and variances σ_a^2 , σ_b^2 . These parameters characterize the smearing and have the following dependence on the polar angle of the parton:

$$\begin{aligned} a_0 &= -0.15 - 0.4 \cos^6 \theta & \sigma_a &= -a_0 \\ b_0 &= 0 & \sigma_b &= 1 \end{aligned}$$

The electron and muon three-momenta were rescaled only in the longitudinal direction by smaller gaussian factors (with $\sigma=0.07$ for e and $\sigma=0.03$ for μ), which were worsened in the forward regions, defined as $\theta < 40^\circ$, $\theta > 140^\circ$, where detection can be less efficient ($\sigma=.1$ for e and $\sigma=.05$ for μ). The parton energies were then rescaled according to the three momentum smearing.

In order to consider only those events which allow acceptable reconstruction, some selection cuts were applied after the smearing: to impose good jet-jet and lepton-jet separation, the minimum angle between two quarks was required to be greater than 5° and the minimum angle between the charged lepton and the jets to be greater than 10° . The minimum invariant mass of jets coming from the same W was 30 GeV. In order then to guarantee the detection of the objects, only partons with polar angle in the region $10^\circ < \theta < 170^\circ$ were considered.

The kinematic constrained fit was then performed on the smeared four-momenta with PUFITC, applying four-momentum conservation and asking for two equal masses in the event. The number of constraints is therefore five for fully hadronic events and two in the mixed hadronic-leptonic ones: in the latter case, in fact, three of the constraints must be used to determine the neutrino direction and momentum. The input errors on jets and leptons for the fit were parametrized in the same way as those used in the smearing procedure.

The effect of requiring equal masses has already been mentioned before: for our purposes, the main result is that the observable to be compared to the fitted mass becomes the average W mass in the event. One must notice that the procedure here described contains other approximations: detector effects leading to non gaussian errors

on jets and leptons are neglected, hard gluon radiation in the final state leading to multi-jet structures and the problem of the correct pairing of the jets in the fully hadronic channel are also ignored. Nevertheless the results we obtain give, in our opinion, a good indication of the effect of a kinematic fit on the mass distributions.

The three curves in fig. 4 show the differential CC20 cross section distributions of the average mass in the event at generator level, after the application of the smearing and after the full reconstruction of the event. The centre-of-mass energy chosen is 172 GeV. It has to be remarked that the $d\sigma/dm$ distribution coming from the constrained fit is a convolution of the generated differential cross-section with the resolution function which, in our case, depends only on parton level smearing. The resolution function is in general a complicated curve whose shape, in principle, depends on the mass itself and on the closeness to the kinematic limit. A test of this will be given in the next section.

Figure 5 presents CC3 $d\sigma/d\bar{m}$ distribution in a different mass range, and the superimposed curves refer to the reconstructed mass distributions in the $q\bar{q}q\bar{q}$ and $q\bar{q}e\nu_e$ channels. One immediately notices the broadening of the two reconstructed curves and the fact that the one for the semileptonic curve is bigger. This difference is basically due to the loss of information caused by the missing neutrino. In the next section we will quantify this difference in terms of shifts in mass and width, trying to separate different contributions to the distortions.

5 Distortions in distributions after constrained fit and their \sqrt{s} dependence.

In this section we study quantitatively the effects described above after the smearing and the reconstruction with the constrained fit.

The reconstruction procedure is not much sensitive to CC20 interference effects. Therefore no marked change, with respect to parton level results, is observed in the CC20-CC3 shifts of the mass and of the width of the distributions. Their value, determined by the difference of the parameters of Breit-Wigner fits to the distributions are reported in table 4, for different values of the centre-of-mass energy. The shifts, about 1.5 times bigger than the ones at generator level of sect. 3, do not depend strongly on ISR and can be considered almost constant in \sqrt{s} .

	172 GeV		184 GeV		200 GeV	
	Δm	$\Delta\Gamma$	Δm	$\Delta\Gamma$	Δm	$\Delta\Gamma$
no ISR	63	19	68	35	63	34
ISR	60	-2	68	5	56	-34

Table 4: Mass and width difference (in MeV) of distributions corresponding to CC20 and CC3 $qqe\nu$ diagrams ($\Delta m = m_{CC20} - m_{CC3}$), for three values of \sqrt{s} , with and without ISR.

Table 5 summarizes the effects of the kinematic reconstruction on the mass distribution in terms of mass and width shifts. From the numbers in the table it turns out that the reconstructed distributions are broader and shifted towards higher masses. There are several causes for this behaviour, as we have discussed in the previous section: missing energy coming from ISR, missing energy coming from the neutrino in the semileptonic channel and intrinsic resolution effects. The latter seem to play a less important role in our framework with respect to the first two, as can be seen from table 5 by comparing the shifts in the fully hadronic channel, no ISR, with the others. The basic effect of pure detector smearing is to broaden the mass distributions, as evident from the $\Delta\Gamma$'s, introducing relatively small biases in the mass. The main contribution to the shift in mass comes from the fact that in the constrained fit the conservation of the energy tends to share the missing ISR energy between the four-momenta in play, increasing the masses in the event. Another interesting information from the table is obtained by comparing corresponding numbers at different centre-of-mass energies: both shift in mass and broadening of the mass distributions increase. This is mainly due to the combined effect of two causes: the first is the increase of the missing ISR energy and the second is that the resolution function which convolves the theoretical $d\sigma/dm$ distribution is broader because the kinematic limit moves away from the resonance and hence the reconstruction error on the mass becomes larger.

		172 GeV		184 GeV		200 GeV	
		Δm	$\Delta\Gamma$	Δm	$\Delta\Gamma$	Δm	$\Delta\Gamma$
$e\bar{\nu}u\bar{d}$	no ISR	51	2083	129	3031	197	3862
	ISR	324	2427	443	3408	523	4234
4q	no ISR	5	757	38	1268	68	1746
	ISR	248	1072	305	1581	353	2069

Table 5: Mass and width difference (in MeV) between reconstructed mass and average generated one ($\Delta m = m_{rec} - m_{gen}$), for three values of \sqrt{s} . The numbers have been determined for $qqqq$ and $qqe\nu$ channels, with and without ISR.

We tried to further quantify the different contributions to the mass distortions: figure 6 shows a comparison between the CC20 average mass distribution produced by WPHACT (continuous line) with the reconstructed ones with (dashed) and without (chaindot) the presence of ISR. The reconstructed mass distribution without ISR has been normalized to the one with ISR. The comparison is interesting because it separates the effect of ISR on neutrino momentum reconstruction and on energy conservation in the fit from the distortions coming from hadronization and detector smearing. In case of presence of ISR, as already discussed, its missing energy is associated to the detected partons and therefore the invariant mass is artificially increased with the result of a shift in mass.

The missing neutrino reconstruction problem is absent in fig. 7, where ISR effect is shown in the reconstruction of the fully hadronic channel. CC3 $d\sigma/d\bar{m}$ true and

reconstructed distributions are compared following the procedure of fig. 6: in this case the difference between the dashed and chain-dot curve represents the ISR effect. As expected the fit of real events (i.e. with ISR) is shifted towards higher value of the mass. The two reconstructed curves also show a difference in width, which is absent between the distributions in fig. 1, because of the extra smearing caused by the undetected ISR energy. The difference in width and mass is studied in table 6, also for other values of \sqrt{s} . The table shows shifts due to the ISR plus the neutrino reconstruction ($qqe\nu$ channel) around 300 MeV for the mass and 350 MeV for the width, while the shifts due to the simple ISR (4q channel) are about 50 MeV lower.

	172 GeV		184 GeV		200 GeV	
	Δm	$\Delta\Gamma$	Δm	$\Delta\Gamma$	Δm	$\Delta\Gamma$
$e\bar{\nu}ud$	247	336	300	376	318	371
4q	218	307	253	312	277	323

Table 6: Mass and width difference (in MeV) between distributions with and without ISR ($\Delta m = m_{ISR} - m_{noISR}$), for three values of \sqrt{s} and for $qqqq$ and $qqe\nu$ channels.

6 Conclusions

We have investigated, from a theoretical point of view, the effects of several approximations on the invariant mass distributions at LEP2 energies. This study is particularly interesting in the light of the first determinations of m_W in LEP experiments using the direct reconstruction technique.

The distortion on the mass distributions have been studied both at generator level and after a simulated reconstruction of the W mass using a constrained fitting method.

Effects coming from CC20 interference, which produces a CC20-CC3 shift of about 40 MeV in $m(e\nu)$ and average distributions at parton level, are dominated by detector resolution, ISR and neutrino missing energy effects after the reconstruction. The interpretation of the single distortions is much more complicated after the kinematic reconstruction because they become strictly connected with each other: ISR is linked to detector inefficiencies and they have, in the case of semileptonic final state, strong effects on neutrino reconstruction.

Our studies, anyway, show that after reconstruction, detector and hadronization effects mainly affect the width of the distributions. The loss of information coming either from undetected ISR or missing neutrino energy has an effect on the mass shift of about 200 MeV and 30 MeV respectively at 172 GeV; the first also contributes to the broadening of the width. The distortions increase with \sqrt{s} . This is due to purely kinematical reasons for detector effects, and in general is a result of the increasing missing energy in the event. This introduces additional complications for a satisfactory determination of m_W , which can be compensated only by a larger statistics.

Acknowledgments

We would like to thank Niels Kjaer, author of PUFITC, for having provided us with the program. We are indebted to Elena Accomando, coauthor of WPHACT, and to Marco Bigi for useful discussions on the arguments of this paper.

References

- [1] Z. Kunszt et al., in Physics at LEP2, G. Altarelli, T. Sjöstrand and F. Zwirner eds., CERN 96-01 (1996), Vol. 1, pg. 141. hep-ph/9602352
- [2] ALEPH Collaboration, *Phys. Lett.* **B401** (1997) 347;
DELPHI Collaboration, *Phys. Lett.* **B397** (1997) 158;
L3 Collaboration, *Phys. Lett.* **B398** (1997) 223;
OPAL Collaboration, *Phys. Lett.* **B389** (1996) 416.
- [3] ALEPH Collaboration, contributed paper nr. 600 to EPS-HEP97;
L3 Collaboration, CERN-PPE/97-98;
OPAL Collaboration, CERN-PPE/97-116.
- [4] DELPHI Collaboration, contributed paper nr. 347 to EPS-HEP97.
- [5] D. Bardin et al., in Physics at LEP2, G. Altarelli, T. Sjöstrand and F. Zwirner eds., CERN 96-01 (1996), Vol. 2, pg 3. hep-ph/9709270
- [6] E. Accomando, A. Ballestrero, G. Passarino, *Nucl. Phys.* **B476** (1996) 3.
- [7] E. Accomando, A. Ballestrero, *Comp. Phys. Commun.* **99** (1997) 270.
- [8] CERN Program library, entry Q121.
- [9] F.A. Berends, R. Pittau and R. Kleiss, *Nucl. Phys.* **B426** (1994) 344;
D. Bardin and T. Riemann, *Nucl. Phys.* **B462** (1996) 3;
T. Ishikawa, Y. Kurihara, M. Skrzypek and Z. Was, prep. CERN-TH/97-11. hep-ph/9702249
- [10] W. Beenakker et al., in Physics at LEP2, G. Altarelli, T. Sjöstrand and F. Zwirner eds., CERN 96-01 (1996), Vol. 1, pg. 79. hep-ph/9612260
- [11] A. Ballestrero, *Acta Phys. Pol.* **B28** (1997) 1445.

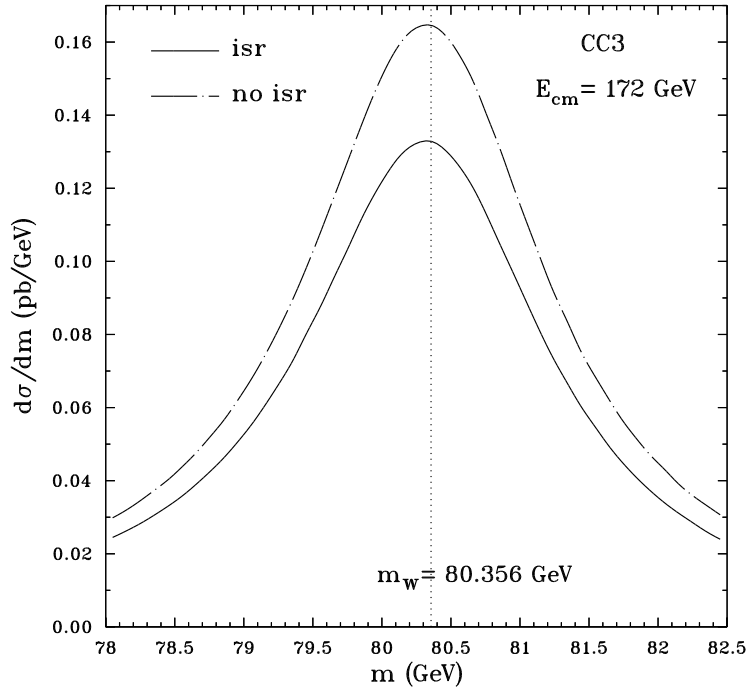


Figure 1: Invariant $u\bar{d}$ mass distribution as given by CC3 diagrams with (continuous) and without (chaindot) ISR.

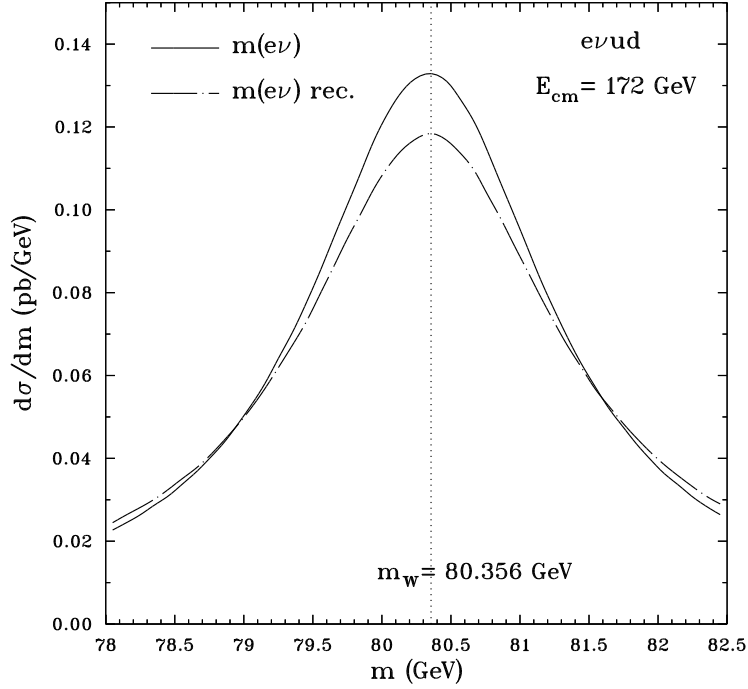


Figure 2: Invariant $e\bar{\nu}$ mass distribution for the complete $e\bar{\nu}u\bar{d}$ process. The continuous line corresponds to the true neutrino momentum, the chaindot to the reconstructed one.

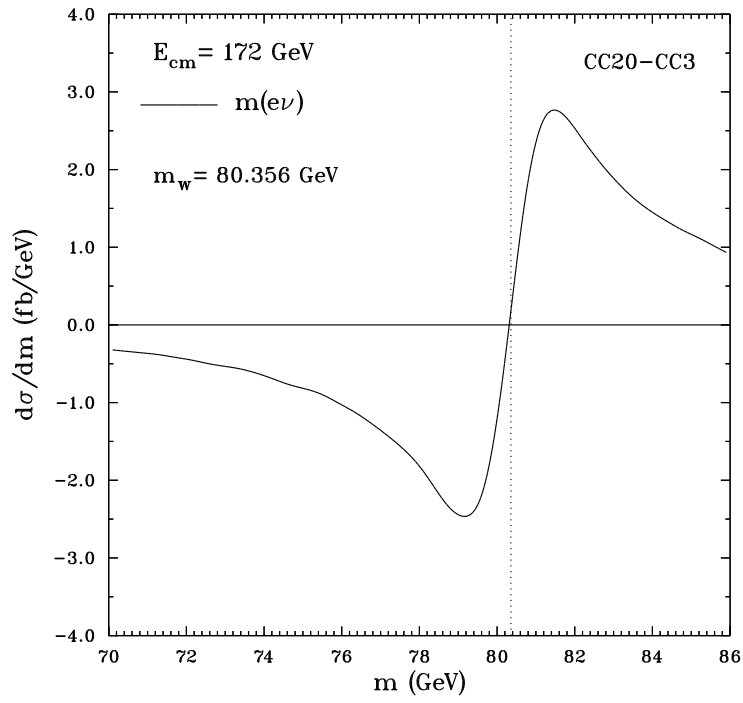


Figure 3: Difference between the invariant $e\bar{\nu}$ mass distribution produced by CC20 and CC3 diagrams.

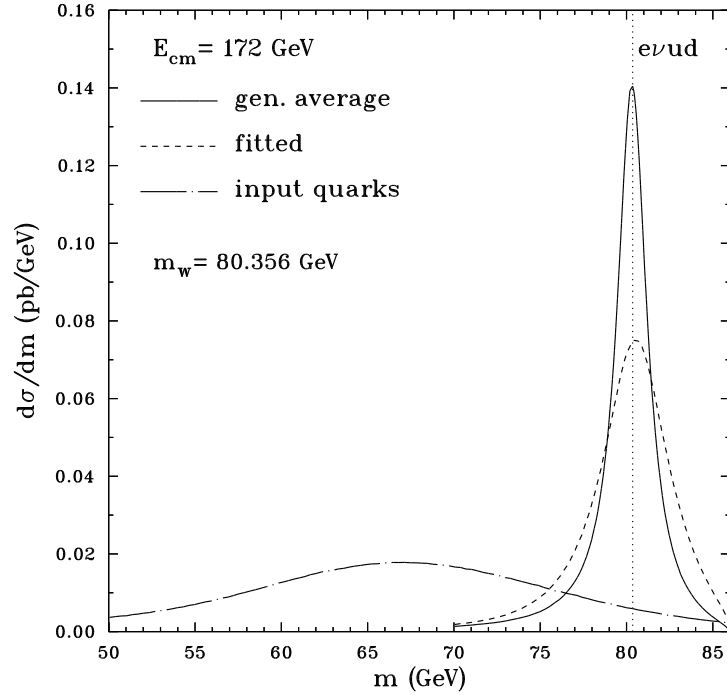


Figure 4: Invariant mass distributions for the complete $e\bar{\nu}u\bar{d}$ process. The continuous line corresponds to the average $(m(e\bar{\nu})+m(u\bar{d}))/2$ mass as generated by WPHACT. The chain-dot one corresponds to $m(u\bar{d})$ after smearing. The dashed line represents the distribution after the kinematical fit done with PUFITC.

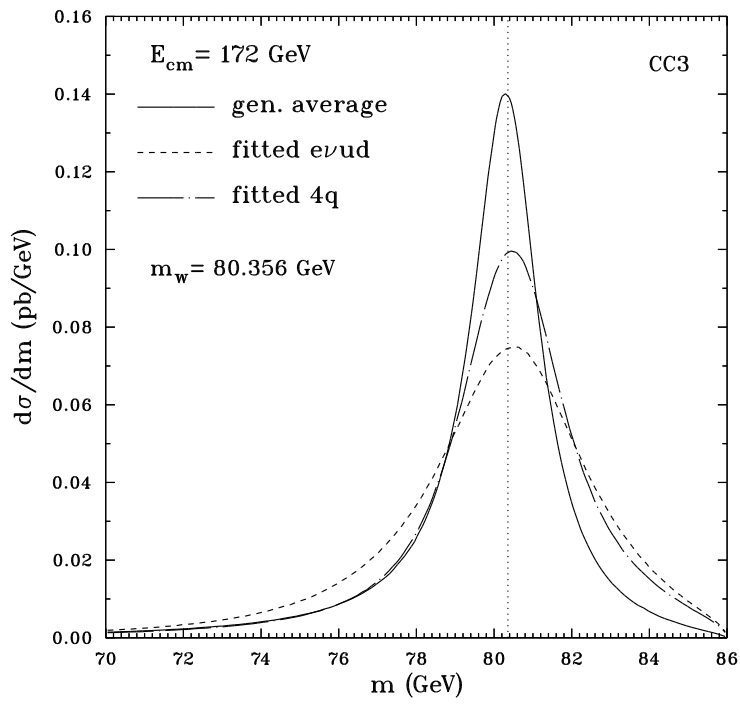


Figure 5: Invariant mass distributions for CC3 contribution. The continuous line corresponds to the average $(m(e\bar{\nu})+m(u\bar{d}))/2$ mass as generated by WPHACT. The dashed line represents the result of the fit with PUFITC for a final $e\bar{\nu}u\bar{d}$ state. The chain-dot one is the result of the same fit for a four quarks finale state.

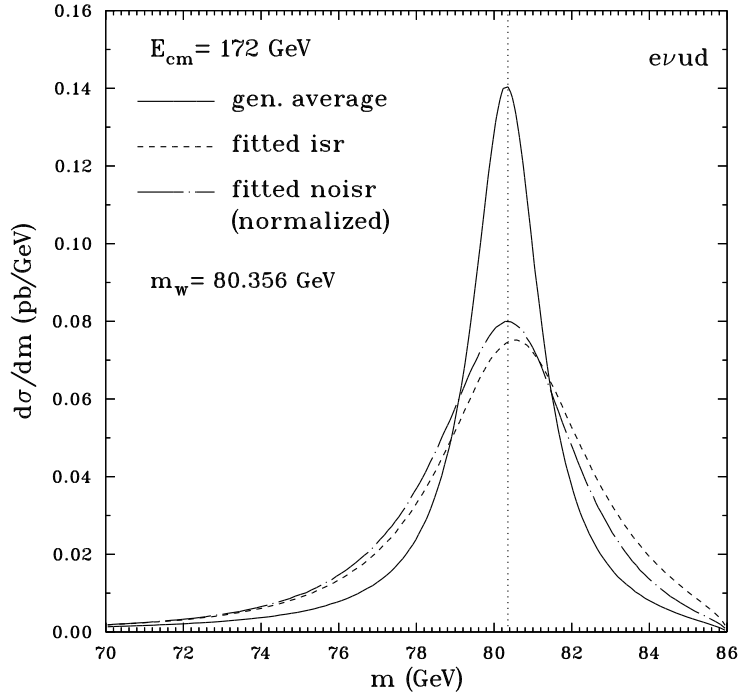


Figure 6: Invariant mass distributions for the complete $e\bar{\nu}u\bar{d}$ process. The continuous line corresponds to the average $(m(e\bar{\nu})+m(u\bar{d}))/2$ mass as generated by WPHACT. The dashed line represents the result of the fit with PUFITC. The chain-dot is the result of the same fit for the process with no ISR, normalized to the ISR one.

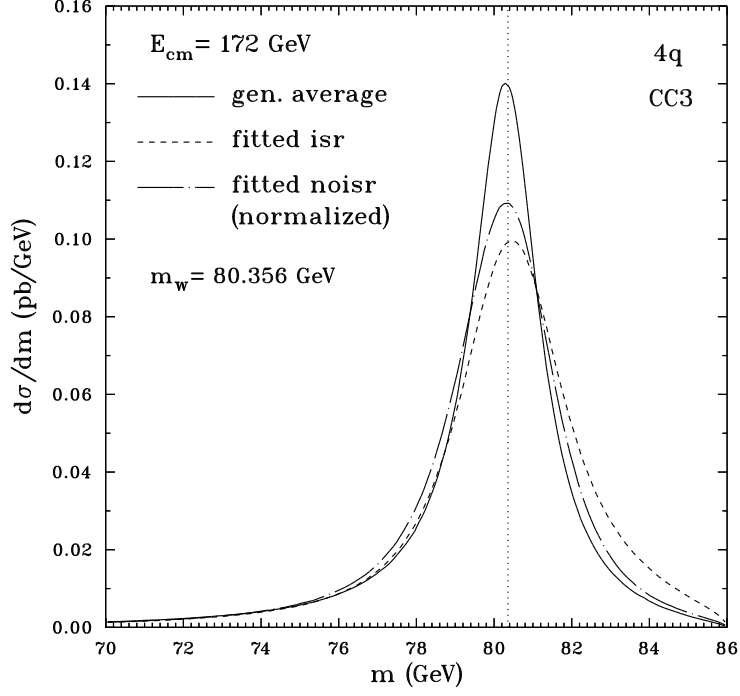


Figure 7: Invariant mass distributions for CC3 contribution in a four quark final state. The continuous line corresponds to the average mass as produced by WPHACT. The dashed line represents the result of the fit with PUFITC. The chain-dot is the result of the same fit for the process with no ISR, normalized to the ISR one.